

Goal-Conditioned End-to-End Visuomotor Control for Versatile Skill Primitives

Oliver Groth¹ Chia-Man Hung¹ Andrea Vedaldi¹ Ingmar Posner¹

Abstract

Visuomotor control (VMC) is an effective means of achieving basic manipulation tasks such as pushing or pick-and-place from raw images. Conditioning VMC on desired goal states is a promising way of achieving versatile *skill primitives*. However, common conditioning schemes either rely on task-specific fine tuning (e.g. using meta-learning) or on sampling approaches using a forward model of scene dynamics i.e. model-predictive control, leaving deployability and planning horizon severely limited. In this paper we propose a conditioning scheme which avoids these pitfalls by learning the controller and its conditioning in an end-to-end manner. Our model predicts complex action sequences based directly on a dynamic image representation of the robot motion and the distance to a given target observation. In contrast to related works, this enables our approach to efficiently perform complex pushing and pick-and-place tasks from raw image observations without predefined control primitives. We report significant improvements in task success over a representative model-predictive controller and also demonstrate our model’s generalisation capabilities in challenging, unseen tasks handling unfamiliar objects.

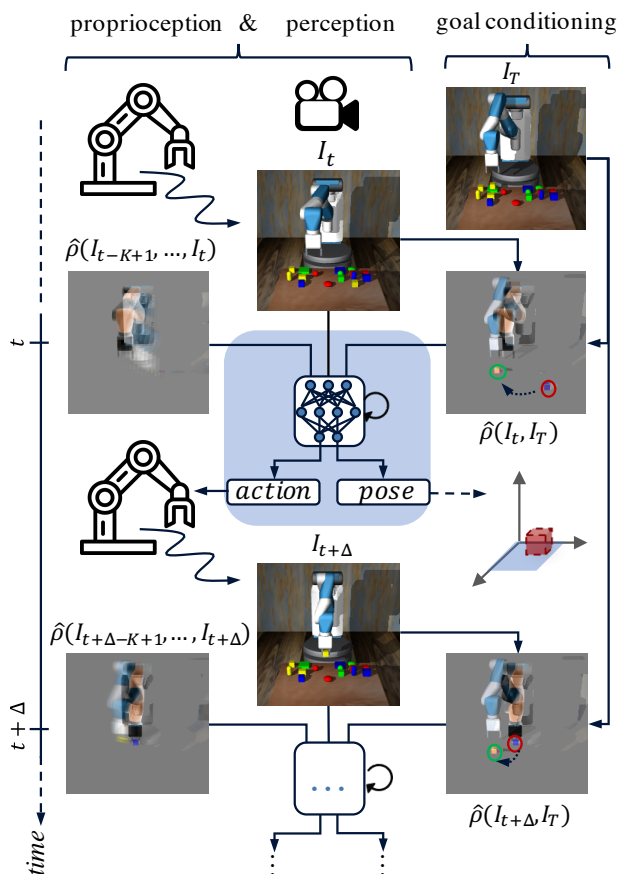


Figure 1. We present a visuomotor controller which can be conditioned on a new task to execute via a target image I_T . In this example, the target image indicates that the small yellow cube from the front right of the table needs to be moved onto the green pad in the back left. Our model uses dynamic images in two places: (1) To represent the difference between its current observation and the target image $\hat{\rho}(I_t, I_T)$ and (2) to capture the motion dynamics $\hat{\rho}(I_{t-K+1}, \dots, I_t)$ during the execution. Current and target location of the object to manipulate are highlighted by red and green circles respectively. The conditioned controller network regresses directly from the observed image stream to motor commands and the pose of the object to move. The figure depicts the controller executing two steps which are Δ time steps apart on a trajectory of accomplishing the task specified in the target image.

1. Introduction

With recent advances in deep learning, we can now learn robotic controllers end-to-end, mapping directly from raw video streams into a robot’s command space. The promise of these approaches is to build real-time visuomotor controllers without the need for complex pipelines or predefined macro-actions (e.g. grasping primitives). End-to-end visuomotor controllers have demonstrated remarkable performance in real systems, e.g. learning to pick up a cube and place it in

¹Department of Engineering Science, University of Oxford, Oxford, United Kingdom. Correspondence to: Oliver Groth <ogroth@robots.ox.ac.uk>.

a basket (James et al., 2017; Zhu et al., 2018). However, a common drawback of current visuomotor controllers is their limited *versatility* due to an often very narrow task definition. For example, in the controllers of (James et al., 2017; Zhu et al., 2018), which are unconditioned, putting a red cube into a blue basket is a different task than putting a yellow cube into a green basket. In contrast to that, in this paper we consider a broader definition of task and argue that it should rather be treated as a *skill primitive* (e.g. a policy which can pick up any object and place it anywhere else). Such a policy must thus be conditioned on certain arguments, e.g. specifying the object to be moved and its target.

Several schemes have been proposed to condition visuomotor controllers on a *target image*, e.g. an image depicting how a scene should look like after the robot has executed its task. Established conditioning schemes build on various approaches such as model-predictive control (Ebert et al., 2018), task-embedding (James et al., 2018) or meta-learning (Finn et al., 2017) and are discussed in greater detail in section 2. However, the different methods rely on costly sampling techniques, access to embeddings of related tasks or task-specific fine-tuning during test time restraining their general applicability.

In contrast to prior work, we propose an efficient end-to-end controller which can be conditioned on a single target image without fine-tuning and regresses directly to motor commands of an actuator without any predefined macro-actions. This allows us to learn general *skill primitives*, e.g. pushing and pick-and-place skills, which are versatile enough to immediately generalise to new tasks, i.e. unseen scene setups and objects to handle. Our model utilises *dynamic images* (Bilen et al., 2017) as a succinct representation of the video dynamics in its observation buffer as well as a visual estimation of the difference between its current observation and the target it is supposed to accomplish. Figure 1 depicts an example execution of our visuomotor controller, its conditioning scheme and intermediate observation representations.

We evaluate our controller on a set of simulated pushing and pick-and-place scenarios in which one object has to be moved to a goal location indicated by a target image. We compare our model against a representative visual model-predictive controller (Ebert et al., 2018) and demonstrate significant improvements in task performance and computational efficiency. We also demonstrate our model’s robustness and versatility by running it in heavily cluttered environments handling unfamiliar objects.

In summary, our contributions are two-fold: Firstly, we propose a novel architecture for visuomotor control which can be efficiently conditioned on a new task with just one single target image. Secondly, we investigate the impact

of the dynamic image representation and show its natural utility at scaling to tasks of varying complexity and dealing with clutter and unseen object geometries for vision-based robotic manipulation.

2. Related Work

The problem of *goal conditioning* constitutes a key challenge in visuomotor control: Given a specific task specification (e.g. putting a red cube onto a blue pad), it needs to be communicated to the robot, which in turn must adapt its control policy in such a way that it can carry out the task. In this paper, we focus on goals which are communicated visually, e.g. through images depicting how objects should be placed on a table. We acknowledge the impressive real-world results which have been achieved in tabletop object rearrangement using pipeline approaches with dedicated perception and planning components (Zagoruyko et al., 2019). However, we restrict the scope of this paper and the related work survey to models which can learn directly from demonstrations or through reinforcement in an end-to-end manner. We group prior work in goal-conditioned VMC by the conditioning scheme being used and the optimisation methods being employed to optimise the action sequences.

In *visual model-predictive control* (MPC) one learns a forward model of the world, forecasting the outcome of an action. A controller samples action sequences and uses the forward model to predict their outcomes, finally choosing the best action sequence under a specific goal distance metric (e.g. image distance in observation space). An established line of work on *Deep Visual Foresight* (VFS) (Finn & Levine, 2017; Ebert et al., 2018; Nair & Finn, 2019; Xie et al., 2019) learns action-conditioned video predictors and employs CEM-like (Rubinstein & Kroese, 2004) sampling methods for trajectory optimisation, successfully applying those models to simulated and real robotic pushing tasks. Another strand of visual MPC focuses on higher-level, object-centric forward modelling as opposed to low-level video prediction for tasks such as block stacking (Ye et al., 2019; Janner et al., 2019). Even though MPC approaches have shown promising results in robot manipulation tasks, they are limited by the quality of the forward model and do not scale well due to the action sampling procedure. In contrast to them, we avoid expensive sampling by directly regressing to the next command given a buffer of previous observations.

To address the challenge of approximating a good distance measure in MPC approaches, another body of work in VMC explores feature or latent spaces which are both suitable for *goal distance* estimation and *control optimisation*. The benefit of those models is their ability to project a goal image and their current observation into their feature space and compute a path towards the target feature for visual servo-

ing (Watter et al., 2015; Byravan et al., 2018), reaching and pushing (Srinivas et al., 2018; Yu et al., 2019) with gradient-based optimisation methods. Visuomotor controllers trained in the reinforcement learning paradigm typically model the distance to a desired, visually specified goal via reward functions which can be either shaped explicitly based on expert domain knowledge (Hundt et al., 2019) or implicitly learned from user feedback about task success (Singh et al., 2019). Our approach of using dynamic images for goal distance estimation sets itself apart from these methods as it uses dynamic images as an efficient, non-parametric conditioning scheme.

One-Shot Imitation Learning seeks to learn general task representations which are quickly adaptable to unseen setups. MIL (Finn et al., 2017) is a meta-controller, which requires fine-tuning during test time on one example demonstration of the new task to adapt to it. In contrast to MIL, TecNet (James et al., 2018) learns a task embedding from expert demonstrations and requires one demonstration of the new task during test time to look up embeddings of similar tasks and modulate its policy accordingly. Additionally, a parallel line of work in that domain operates on discrete action spaces (Xu et al., 2018; Huang et al., 2019) and maps demonstrations of new tasks to known macro actions. Unlike those methods, our model is conditioned on a single target image and does not require any fine-tuning on a new task during test time.

3. Goal-Conditioned Visuomotor Control

In order to build a visuomotor controller which can be efficiently conditioned on a target image and is versatile enough to generalise its learned policy to new tasks immediately, we need to address the following problems: Firstly, we need an efficient way to detect scene changes, i.e. answering the question ‘Which object has been moved and where from and to?’ Secondly, we want to filter our raw visual observation stream such that we only retain information pertinent to the control task; specifically the motion dynamics of the robot as well as the poses of the end effector (i.e. the robot’s gripper) and the manipulated object. Drawing inspiration from previous work in VMC and action recognition, we propose *GEECO*, a novel architecture for *goal-conditioned end-to-end control* which combines the idea of *dynamic images* (Bilen et al., 2017) with a robust end-to-end controller network (James et al., 2017) to learn versatile manipulation skill primitives which can be conditioned on new tasks on the fly. We discuss next the individual components.

Dynamic Images. In the domain of action recognition, dynamic images have been developed as a succinct video representation capturing the dynamics of an entire frame sequence in a single image. This enables the treatment of a video with convolutional neural networks as if it was an

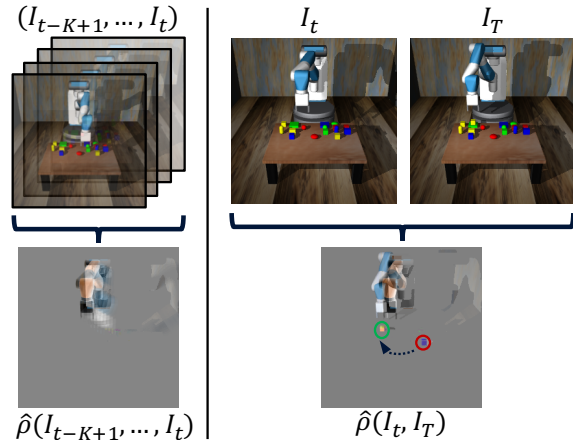


Figure 2. Utilisation of dynamic images. Left: A dynamic image represents the motion occurring in a sequence of K consecutive RGB observations. Right: A dynamic image represents the changes which occurred between the two images I_t and I_T like the change of object positions as indicated by the red and green circles. In both cases, the representation specifically captures geometric details changing between frames and cancels out all static parts.

ordinary RGB image facilitating dynamics-related feature extraction. The core of the dynamic image representation is a ranking machine which learns to sort the frames of a video temporally (Fernando et al., 2015). As shown by prior work (Bilen et al., 2017), an approximate linear ranking operator $\hat{\rho}(\cdot)$ can be applied to any sequence of H temporally ordered frames (I_1, \dots, I_H) and any image feature extraction function $\psi(\cdot)$ to obtain a dynamic feature map according to the following eqs. (1) and (2):

$$\hat{\rho}(I_1, \dots, I_H; \psi) = \sum_{t=1}^H \alpha_t \psi(I_t) \quad (1)$$

$$\alpha_t = 2(H - t + 1) - (H + 1)(\mathcal{H}_H - \mathcal{H}_{t-1}) \quad (2)$$

Here, $\mathcal{H}_t = \sum_{i=1}^t 1/i$ is the t -th Harmonic number and $\mathcal{H}_0 = 0$. Setting $\psi(\cdot)$ to the identity, $\hat{\rho}(I_1, \dots, I_H)$ yields a dynamic image which, after normalisation across all channels, can be treated as a normal RGB image by a downstream network. The employment of dynamic images chiefly serves two purposes in our network, as depicted in fig. 2. Firstly, it compresses a window of the last K RGB observations into one image $\hat{\rho}(I_{t-K+1}, \dots, I_t)$ capturing the current motion of the robot arm. Secondly, given a target image I_T depicting the final state the scene should be in, the dynamic image $\hat{\rho}(I_t, I_T)$ lends itself very naturally to represent the *visual difference* between the current observation I_t and the target state I_T . Another advantage of using dynamic images in these two places is to make the controller network invariant w.r.t. the static scene background and, approximately, the object colour, allowing it to focus on location and geometry of objects involved in the manipulation task.

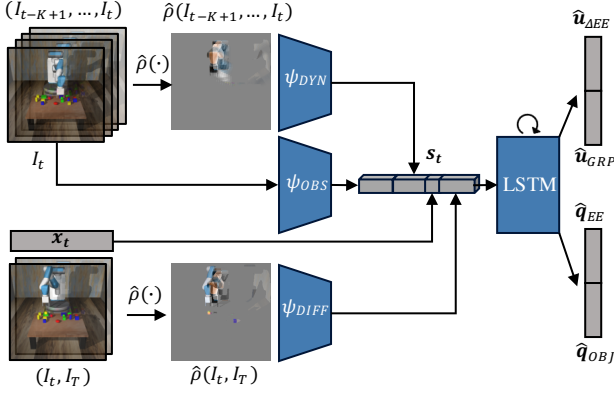


Figure 3. Network architecture of our full model: GEECO_F. The images (I_{t-K+1}, \dots, I_T) of the observation buffer are compressed into a dynamic image via $\hat{\rho}(\cdot)$ and passed on to a CNN ψ_{DYN} . The difference between the current observation I_t and the target frame I_T is also computed via $\hat{\rho}(\cdot)$ and passed through a separate CNN ψ_{DIFF} . Lastly, the current observation I_t is passed through another CNN ψ_{OBS} . All CNNs compute spatial feature maps which are concatenated to the tiled proprioceptive feature \mathbf{x}_t . The concatenated state representation \mathbf{s}_t is fed into an LSTM whose output is decoded into command actions $\hat{\mathbf{u}}_{\Delta EE}$ and $\hat{\mathbf{u}}_{GRP}$ as well as auxiliary pose predictions $\hat{\mathbf{q}}_{EE}$ and $\hat{\mathbf{q}}_{OBJ}$. The full model operates with a frame buffer size of $K = 4$ on RGB images of 256×256 pixels and contains approx. 7.6M trainable parameters.

Observation Buffer. During execution, our network maintains a buffer of most recent K observations as a sequence of pairs $((I_{t-K+1}, \mathbf{x}_{t-K+1}), \dots, (I_t, \mathbf{x}_t))$ where I_t is the RGB frame at time step t and \mathbf{x}_t is the proprioceptive feature of the robot at the same time step represented as a vector of its joint angles. Having the controller network only regress to the next action based on a short observation buffer makes it more akin to a greedy reflex. However, it also adds robustness, breaking long-horizon manipulation trajectories into shorter windows which retain relative independence from each other. This endows the controller with a certain error-correction capacity, e.g. when a grasped object slips from the gripper prematurely, the network naturally regresses back to a pick-up phase.

Goal Conditioning. Before executing a trajectory, our controller is *conditioned* on the task to execute, i.e. moving an object from its initial position to a goal position, via a target image I_T depicting the scene after the task has been carried out. Given this task specification, the controller then faces two challenges: identifying the object to manipulate and identifying the target location. As shown in fig. 2 (right), the dynamic image representation $\hat{\rho}(I_t, I_T)$ helps this inference process by only retaining the two object positions and the difference in the robot pose while cancelling out all static parts of the scene.

Network Architecture. The controller network takes the current observation buffer $((I_{t-K+1}, \mathbf{x}_{t-K+1}), \dots, (I_t, \mathbf{x}_t))$ and the target image I_T as input and regresses to the following two action outputs: (1) The change in Cartesian coordinates of the end effector $\hat{\mathbf{u}}_{\Delta EE}$ and (2) a discrete signal $\hat{\mathbf{u}}_{GRP}$ for the gripper to either open (-1), close ($+1$) or stay in position (0). Additionally, the controller regresses two auxiliary outputs: The current position of the end effector $\hat{\mathbf{q}}_{EE}$ and of the object to manipulate $\hat{\mathbf{q}}_{OBJ}$, both in absolute Cartesian world coordinates. While the action vectors $\hat{\mathbf{u}}_{\Delta EE}$ and $\hat{\mathbf{u}}_{GRP}$ are directly used to control the robot, the position predictions serve as an auxiliary signal during the supervised training process to encourage the network to learn intermediate representations correlated to the world coordinates.

The model architecture is based on E2EVMC (James et al., 2017), a robust network for end-to-end visuomotor control whose efficacy has been demonstrated in simulated and real world manipulation settings. We extend E2EVMC by processing the observation buffer as a dynamic image instead of as a sequence of individual frames. We also add a separate convolutional branch for goal conditioning. A sketch of our model architecture can be found in fig. 3 and we refer the reader to the appendix of this paper for a detailed description of all architectural parameters.

The full model is trained in an end-to-end fashion on N expert demonstrations of manipulation tasks collected in a simulation environment. Each expert demonstration is a sequence of H time steps indexed by t containing: the RGB frame I_t , the proprioceptive feature \mathbf{x}_t , the robot commands $\mathbf{u}_{\Delta EE}^*(t)$, $\mathbf{u}_{GRP}^*(t)$ and the positions of the end effector and the object to manipulate $\mathbf{q}_{EE}^*(t)$, $\mathbf{q}_{OBJ}^*(t)$. During training, we minimise the following loss function:

$$\mathcal{L} = \sum_{i=1}^N \left[\sum_{t=1}^{H-K+1} \text{MSE}(\hat{\mathbf{u}}_{\Delta EE}(\tau_{i,t}), \mathbf{u}_{\Delta EE}^*(i,t)) + \text{Softmax}(\hat{\mathbf{u}}_{GRP}(\tau_{i,t}), \mathbf{u}_{GRP}^*(i,t)) + \text{MSE}(\hat{\mathbf{q}}_{EE}(\tau_{i,t}), \mathbf{q}_{EE}^*(i,t)) + \text{MSE}(\hat{\mathbf{q}}_{OBJ}(\tau_{i,t}), \mathbf{q}_{OBJ}^*(i,t)) \right] \quad (3)$$

The shorthand notation $\tau_{i,t}$ represents the t -th training window in the i -th expert demonstration of the training dataset comprising of $((I_t, \mathbf{x}_t), \dots, (I_{t+K-1}, \mathbf{x}_{t+K-1}))$; $I_T = I_H$; $\mathbf{u}^*(i,t)$ and $\mathbf{q}^*(i,t)$ are the corresponding ground truth commands, and $\hat{\mathbf{u}}(\cdot)$ and $\hat{\mathbf{q}}(\cdot)$ are shorthand notations for the network predictions on that window. During training we always set the target frame I_T to be the last frame of the expert demonstration I_H .

Model Ablations. We refer to our *full* model as $\text{GEECO}_{\mathcal{F}}$ as depicted in fig. 3. However, in order to gauge the effectiveness of the dynamic image representations, we also consider three ablations of our proposed model utilising dynamic images to a different degree or not at all.

$\text{GEECO}_{\mathcal{C}}$ (approx. 2.6M parameters): The CNNs ψ_{DYN} and ψ_{DIFF} are removed from $\text{GEECO}_{\mathcal{F}}$ and only ψ_{OBS} is retained. The target image I_T is passed through ψ_{OBS} and its feature is concatenated to the one obtained from the current observation I_t and the proprioceptive feature \mathbf{x}_t yielding the state feature \mathbf{s}_t . This is a naive baseline for goal conditioning gauging whether the conditioning problem can be solved by a simple concatenation of a *constant* target feature.

$\text{GEECO}_{\mathcal{R}}$ (approx. 2.6M parameters): This ablation also has ψ_{DYN} and ψ_{DIFF} removed like $\text{GEECO}_{\mathcal{C}}$ and ψ_{OBS} is responsible for encoding both the current observation I_t and the target image I_T . However, instead of simply concatenating the respective features, this model computes their difference and uses it in the state feature \mathbf{s}_t . This *residual* state encoding encourages the model to learn meaningful goal distances in the feature space induced by ψ_{OBS} and serves as a baseline for an implicitly learned goal distance.

$\text{GEECO}_{\mathcal{D}}$ (approx. 5.1M parameters): The *dynamic difference* $\hat{\rho}(I_t, I_T)$ is computed at each time step and passed through ψ_{DIFF} . The RGB observations are also encoded via ψ_{OBS} . The features obtained from ψ_{OBS} and ψ_{DIFF} are concatenated to \mathbf{x}_t forming the state representation \mathbf{s}_t . This ablation gauges the effectiveness of using an explicitly shaped goal difference function over an implicitly learned one like in $\text{GEECO}_{\mathcal{R}}$.

4. Experiments

The experimental design and evaluation of our model are guided by the following three questions: (1) How well can our model learn skill primitives for pushing and pick-and-place tasks in a simulated tabletop environment and how does it compare to a representative approach of visual MPC? (2) How well can our network cope with the multi-stage nature of the control problem, i.e. inferring the object to manipulate, reaching it and putting it into the inferred goal location? (3) How well does our controller generalise when employed in settings beyond the training setup featuring many more objects and previously unseen geometries?

Experimental Setup and Data Collection. We have designed four different simulation scenarios to train and evaluate our controller models which are presented in fig. 4. Each scenario is designed to probe one specific aspect of the controller: GOAL1CUBE1 is modelled after similar experiments in prior work (James et al., 2017; Zhu et al., 2018) where one cube has to be moved on top of a designated

goal object. This scenario can already be solved by an unconditioned controller simply executing a narrow policy of placing a red object on top of a blue one and allows a fair comparison with previous approaches. GOAL1CUBE2 and GOAL2CUBE1 represent both sides of the goal-conditioning problem: GOAL1CUBE2 requires identifying the correct object to manipulate while GOAL2CUBE1 conversely focuses on the identification of the goal position. Finally, GOAL2CUBE2 combines both aspects and requires the controller to identify object and goal while disregarding distractors.

We use the MuJoCo physics engine (Todorov et al., 2012) to simulate all scenarios. We adapt the Gym environment (Brockman et al., 2016) provided by (Duan et al., 2017) featuring a model of a *Fetch Mobile Manipulator* (Wise et al., 2018) with a 7-DoF arm and a 2-point gripper to execute the tasks¹. The robot’s action space consists of a three-dimensional vector $\mathbf{u}_{\Delta EE}$ controlling the end effector position in Cartesian space and a discrete command \mathbf{u}_{GRP} indicating the gripper mode. For each scenario and each skill, i.e. pushing and pick-and-place, we collect 4,000 unique expert demonstrations of the robot completing the task successfully in simulation according to a pre-computed plan. *Uniqueness* is defined as a unique combination of the initial poses of all objects and the robot. Each demonstration is 4 seconds long and is recorded as a list of observation-action tuples (cf. section 3) at 25 Hz resulting in an episode length of $H = 100$.

Baseline for Goal-Conditioned VMC. We choose VFS (Ebert et al., 2018) as a representative goal-conditioned baseline from the paradigm of visual MPC (cf. section 2). We use the official implementation of SAVP (Lee et al., 2018) as its backbone for action-conditioned video prediction and train it on our datasets with the hyper-parameters reported for the BAIR robot-pushing dataset (Ebert et al., 2017) as it is most akin to our use case. For computational reasons, we reduce the resolution of SAVP to 128×128 pixels to run it alongside the physics engine during test time. In order to employ VFS in our scenarios, we need to extend its action space to three Cartesian dimensions as opposed to two in the original implementation. Since this extended action space increases the difficulty of sampling correct trajectories, we resort to providing intermediate target images to VFS taken from an expert demonstration to estimate an upper bound of the model’s performance when it only needs to predict approximately linear sub-trajectories². We refer the reader to the appendix for a complete summary of VFS’s hyper-parameter setup during deployment.

¹Despite the robot having a mobile platform, its base is fixed during all experiments.

²HVF (Nair & Finn, 2019) employs a similar ‘ground truth bottleneck’ scheme to upper-bound a visual MPC baseline.

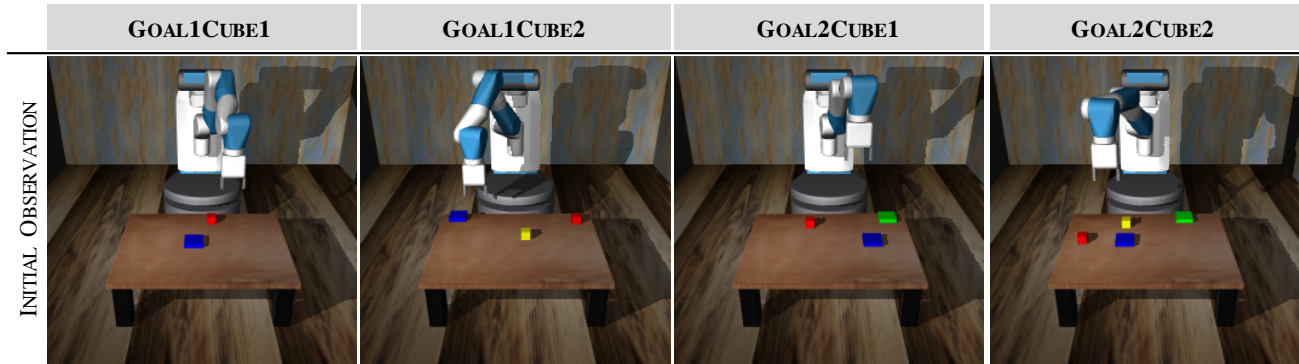


Figure 4. Overview of the basic scenarios used during experimentation. GOAL1CUBE1: One red cube needs to be moved onto the blue target pad. GOAL1CUBE2: Either of the two cubes needs to be moved onto the target pad. GOAL2CUBE1: The cube needs to be moved onto either of the two target pads. GOAL2CUBE2: One cube needs to go on top of one target pad. In each scenario, the objects are exactly the same for each recorded episode and only their initial positions and the initial pose of the robot arm are randomised.

Training Protocol. We randomly split each dataset of demonstrations into training, validation and test sets with a ratio of 5 : 3 : 2 respectively. We train SAVP and all versions of GEECO for 300k gradient update steps using the Adam optimiser (Kingma & Ba, 2015) with a start learning rate of $1e-4$. SAVP and GEECO are trained on each of our eight datasets individually. In the case of SAVP, we select the model checkpoint after 300k iterations for the final evaluation. In the case of GEECO, we always select the latest model checkpoint from the top-10 ones with the lowest validation set loss. The rationale behind this model selection is the observation that controllers which have been trained for more than 200k steps are generally more robust during execution despite slightly higher losses on the validation set than the ones at ‘overfitting point’.

Evaluation Protocol. We evaluate all controllers in simulation on held-out test setups of our datasets. During task execution, we monitor the following performance metrics:

Reach: If the robot touches the object it is supposed to manipulate at least once during the episode, we count this as a reaching success.

Pick: If the palm of the robot’s gripper touches the correct object at least once during the episode while the fingers are closed, we count this as a picking success.

Push / Place: If by the end of the episode the correct object sits on the designated goal pad, we count this as task success in the respective skill.

Goal Distance Reduction: At the end of each episode, we report the final ratio of how much the controller managed to reduce the distance of the correct object to its designated goal location compared to the distance at the start of the episode.

Each evaluation episode is terminated after 200 timesteps

(8 seconds). The extended episode length compared to the expert demonstrations gives the controllers a fair chance, even when executing imperfect actions, and allows them to recover from failures (e.g. when dropping an object prematurely).

Manipulation Results in Basic Scenarios. Our four basic scenarios are specifically designed to address our first two guiding questions: How does our method compare against a model-predictive controller trained under the same conditions and how does it handle the different aspects of conditioning? For skills, i.e. pushing and pick-and-place, we evaluate the performance of the controllers on 100 held-out scene setups from the respective test sets of each scenario. We calibrate the task performance on the test sets against RAND, a controller which samples actions according to a multivariate Normal distribution over the action space to estimate the task difficulty.

We report success performances for all pushing tasks in table 1 and for all pick-and-place tasks in table 2. For a more nuanced performance analysis beyond the binary success indicators, we also report the distributions of the models’ goal distance reduction metric as boxplots in fig. 5.

On pushing tasks, all versions of GEECO exhibit nearly perfect reaching performance significantly outperforming VFS by a margin of at least 20%. The positive outliers of VFS on pushing tasks in fig. 5 indicate several successful pushes towards the target pads. However, the boxplot median usually rests around zero indicating that VFS struggles to maintain a stable push after reaching the right object resulting in all episodes timing out before the target pads have been reached. In terms of task success, our ‘RGB-only’ ablations GEECO_C and GEECO_R are on-par with or occasionally even better than GEECO_D and GEECO_F using dynamic images. However, as fig. 5 reveals, the ‘dynamic’ models

MODEL	GOAL1CUBE1		GOAL1CUBE2		GOAL2CUBE1		GOAL2CUBE2	
	REACH [%]	PUSH [%]						
RAND	6	2	4	12	7	8	0	12
VFS	56	2	69	11	37	8	66	7
GEECO _C	98	64	97	71	97	67	99	82
GEECO _R	98	42	100	67	99	73	99	55
GEECO _D	98	68	99	82	99	87	100	70
GEECO _F	100	55	98	67	100	86	99	42

Table 1. Reaching and pushing success rate in the four basic scenarios. Each success rate is computed based on 100 trials from the scenario’s respective test set. Higher PUSH than REACH rates can occur when objects are already spawned on their target pads.

MODEL	GOAL1CUBE1			GOAL1CUBE2			GOAL2CUBE1			GOAL2CUBE2		
	REACH [%]	PICK [%]	PLACE [%]	REACH [%]	PICK [%]	PLACE [%]	REACH [%]	PICK [%]	PLACE [%]	REACH [%]	PICK [%]	PLACE [%]
RAND	6	2	0	7	1	0	7	0	0	8	1	0
VFS	79	17	0	91	23	0	92	31	0	87	40	0
GEECO _C	98	84	56	69	38	20	97	81	64	53	22	6
GEECO _R	94	58	47	91	62	39	96	73	47	87	54	33
GEECO _D	98	89	54	94	71	44	96	73	39	98	80	41
GEECO _F	96	80	79	94	56	41	99	89	51	94	86	31

Table 2. Reaching, picking and placing success rates in the four basic scenarios. Each success rate is computed based on 100 trials from the scenario’s respective test set.

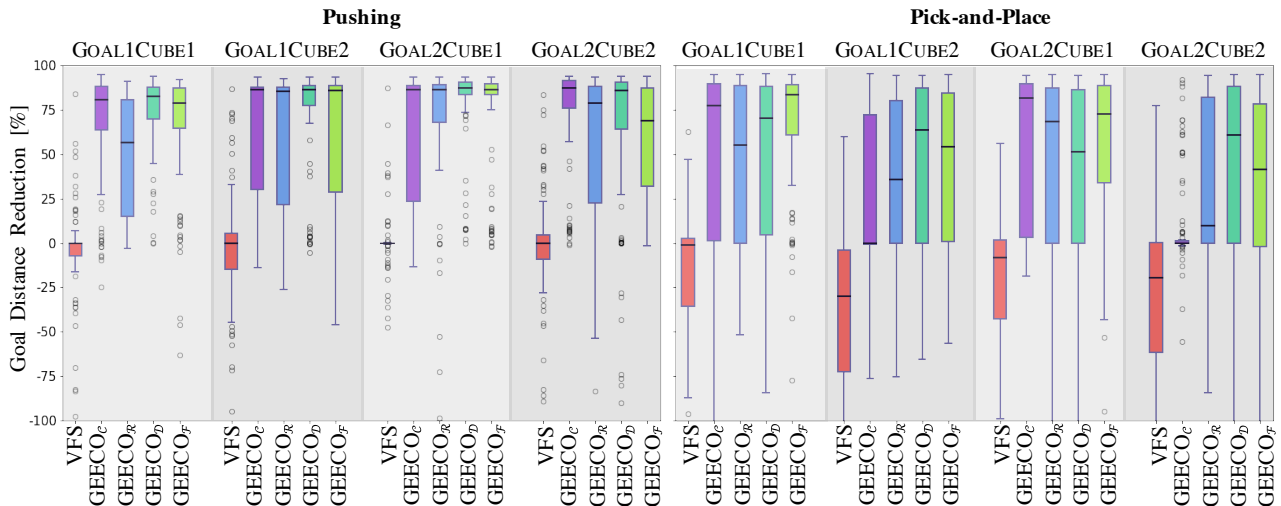


Figure 5. Goal distance reduction in the four basic scenarios for pushing and pick-and-place tasks across all evaluation runs of VFS and all versions of GEECO. 100% indicates the cube being perfectly moved onto the target pad; negative values indicate the cube being moved away from its designated target. Outliers below -100% are cropped. High negative scores can occur in failure cases when objects are accidentally knocked off the table.

consistently maintain higher performance and lower spread in distance reduction, indicating that especially the goal conditioning with dynamic images (GEECO_D) contributes significantly to the success of the planar pushing task.

In the pick-and-place tasks, VFS catches up to GEECO_C in reaching and picking performance, even outperforming it on GOAL2CUBE2. This is surprising given that pick-and-place is supposedly a harder task than pushing. We conjecture that this stems from the higher complexity of the trajectories in the pick-and-place demonstrations helping the video predictor to learn a more accurate forward dynamics model. However, VFS’s sampling-driven, erratic movement makes it impossible to maintain a stable grasp resulting in 0% placing performance across the board. The boxplots for VFS in fig. 5 add evidence for this failure mode: They report the majority of goal-distance reductions in the pick-and-place tasks below zero indicating that VFS moves objects erratically and mostly in the wrong direction. This suggests that a multi-stage task with a complex motion trajectory is probably beyond the limits of what visual MPC can accomplish without significant model additions for sub-goal and target difference estimation. Analysing GEECO’s performance on pick-and-place tasks, we observe a significant drop in reaching success of GEECO_C in scenarios involving two potential cubes to manipulate indicating that the naïve concatenation of a static target feature is not helpful during the stage of object identification. In contrast, we consistently observe a strong reaching and picking success of GEECO_D across all scenarios adding further evidence of the benefit provided by the dynamic image for object identification and goal inference.

Qualitatively, we also observe interesting behaviours of all GEECO ablations across all skills and scenarios³. If our controller makes a mistake (e.g. moving slightly past an object or dropping it prematurely), it automatically regresses back to a pick-up-phase despite having never seen *any* error-prone demonstration during training. This highlights the reflex character of our model but also showcases its inherent robustness despite the supervised learning paradigm. GEECO_F also exhibits smoother and less erratic movements than its ablations without the dynamic image frame buffer compression suggesting its utility towards nuanced motions but also leading to task ‘failures’ of too slow execution, i.e. the episode terminates in the middle of an otherwise successful execution. Other failure modes like pushing an object outside of the gripper range or getting stuck in an imprecise re-grasping loop largely stem from the model’s limited perception of 3D and could probably be remedied by adding a depth sensor to the setup.

³A video depicting qualitative examples of the controller execution as well as common success and failure modes is provided at <https://youtu.be/zn.lPor9zCU>

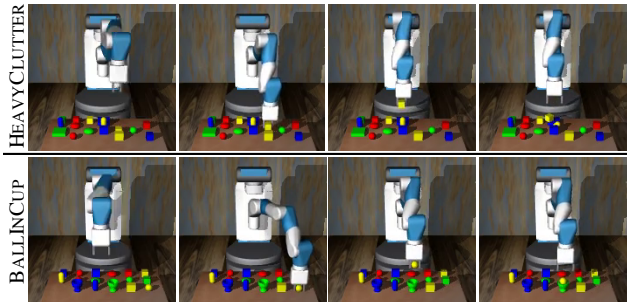


Figure 6. GEECO_F successfully completes tasks in heavy clutter involving object geometries it has never been trained on. Top row: Executing a GOAL2CUBE2 task under the presence of 12 clutter objects. Bottom row: Placing a ball in a cup. Images are centre-cropped for better visibility.

Generalisation to New Scenarios. Beyond the four basic scenarios, we create two additional pick-and-place test sets of 100 scene setups each to answer our third guiding question and gauge the generalisation capabilities of GEECO. Transferring a learned skill to a new scenario is a key quality of the *versatility* we hope to achieve with our architecture. Both scenarios, HEAVYCLUTTER and BALLINCUP are variations of GOAL2CUBE2. However, both scenarios also contain 12 additional objects of seen (boxes) and unseen geometries (capsules, balls, ellipsoids) cluttering the table. Additionally, BALLINCUP also changes the task setup depicting balls which need to be placed in cups - two object geometries GEECO has never interacted with during training on GOAL2CUBE2.

MODEL	HEAVYCLUTTER			BALLINCUP		
	REACH [%]	PICK [%]	PLACE [%]	REACH [%]	PICK [%]	PLACE [%]
RAND	12	0	0	8	2	0
GEECO _C	12	3	0	5	0	0
GEECO _R	62	29	18	15	5	0
GEECO _D	75	52	27	55	9	0
GEECO _F	83	56	23	59	20	1

Table 3. Pick-and-place performance of models trained on GOAL2CUBE2 and employed in heavily cluttered scenarios.

Our experiments show that GEECO_C breaks completely when facing unseen scenarios and the rapidly dropping success of GEECO_R indicates the limitations of the feature space measuring task distance, especially when handling unseen objects in BALLINCUP. Remarkably, GEECO_F maintains a high reaching and decent picking performance even when handling balls demonstrating the benefit of the dynamic image encoding of the frame buffer over GEECO_D for more nuanced motions.

5. Conclusions

We introduce GEECO, a novel architecture for goal-conditioned end-to-end visuomotor control utilising dynamic images. GEECO can be immediately conditioned on a new task with the input of a single target image. Leveraging dynamic images, it solves both aspects of conditioning (i.e. object and goal identification) robustly and efficiently. We demonstrate GEECO’s efficacy in complex pushing and pick-and-place tasks involving multiple objects. It also generalises well to challenging, unseen scenarios maintaining strong task performance even in heavy clutter and while handling novel object geometries. Additionally, its built-in invariances can also help reduce the dependency on sophisticated randomisation schemes during the training of visuomotor controllers. Our results suggest that GEECO can serve as a robust component in robotic manipulation tasks enabling the re-use of versatile skill primitives.

Acknowledgements

Oliver Groth is funded by the European Research Council under grant ERC 677195-IDIU. Chia-Man Hung is funded by the Clarendon Fund and receives a Keble College Sloane Robinson Scholarship at the University of Oxford. This work is also supported by an EPSRC Programme Grant (EP/M019918/1). The authors acknowledge the use of Hartree Centre resources in this work. The STFC Hartree Centre is a research collaboratory in association with IBM providing High Performance Computing platforms funded by the UK’s investment in e-Infrastructure. The authors also acknowledge the use of the University of Oxford Advanced Research Computing (ARC) facility in carrying out this work (<http://dx.doi.org/10.5281/zenodo.22558>). Special thanks goes to Frederik Ebert for his helpful advise on adjusting Visual Foresight to our scenarios and to Ștefan Săftescu for lending a hand in managing experiments on the compute clusters. Lastly, we would also like to thank our dear colleagues Martin Engelcke, Sudhanshu Kasewa, Christian Rupprecht, Sébastien Ehrhardt and Olivia Wiles for proofreading and their helpful suggestions and discussions on this draft.

References

- Bilen, H., Fernando, B., Gavves, E., and Vedaldi, A. Action recognition with dynamic image networks. *IEEE transactions on pattern analysis and machine intelligence*, 40 (12):2799–2813, 2017.
- Brockman, G., Cheung, V., Pettersson, L., Schneider, J., Schulman, J., Tang, J., and Zaremba, W. Openai gym, 2016.
- Byravan, A., Lceb, F., Meier, F., and Fox, D. Se3-pose-nets: Structured deep dynamics models for visuomotor control. In *2018 IEEE International Conference on Robotics and Automation (ICRA)*, pp. 1–8. IEEE, 2018.
- Duan, Y., Andrychowicz, M., Stadie, B., Ho, O. J., Schneider, J., Sutskever, I., Abbeel, P., and Zaremba, W. One-shot imitation learning. In *Advances in neural information processing systems*, pp. 1087–1098, 2017.
- Ebert, F., Finn, C., Lee, A. X., and Levine, S. Self-supervised visual planning with temporal skip connections. In *Conference on Robot Learning*, 2017.
- Ebert, F., Finn, C., Dasari, S., Xie, A., Lee, A., and Levine, S. Visual foresight: Model-based deep reinforcement learning for vision-based robotic control. *arXiv preprint arXiv:1812.00568*, 2018.
- Fernando, B., Gavves, E., Jos Oramas, M., Ghodrati, A., and Tuytelaars, T. Modeling video evolution for action recognition. In *2015 IEEE Conference on Computer Vision and Pattern Recognition (CVPR)*, pp. 5378–5387, June 2015. doi: 10.1109/CVPR.2015.7299176.
- Finn, C. and Levine, S. Deep visual foresight for planning robot motion. In *2017 IEEE International Conference on Robotics and Automation (ICRA)*, pp. 2786–2793, May 2017. doi: 10.1109/ICRA.2017.7989324.
- Finn, C., Yu, T., Zhang, T., Abbeel, P., and Levine, S. One-shot visual imitation learning via meta-learning. In *Conference on Robot Learning*, pp. 357–368, 2017.
- Huang, D.-A., Nair, S., Xu, D., Zhu, Y., Garg, A., Fei-Fei, L., Savarese, S., and Niebles, J. C. Neural task graphs: Generalizing to unseen tasks from a single video demonstration. In *Proceedings of the IEEE Conference on Computer Vision and Pattern Recognition*, pp. 8565–8574, 2019.
- Hundt, A., Killeen, B., Kwon, H., Paxton, C., and Hager, G. D. ” good robot! ”: Efficient reinforcement learning for multi-step visual tasks via reward shaping. *arXiv preprint arXiv:1909.11730*, 2019.

- James, S., Davison, A. J., and Johns, E. Transferring end-to-end visuomotor control from simulation to real world for a multi-stage task. In *Conference on Robot Learning*, pp. 334–343, 2017.
- James, S., Bloesch, M., and Davison, A. J. Task-embedded control networks for few-shot imitation learning. In *Conference on Robot Learning*, pp. 783–795, 2018.
- Janner, M., Levine, S., Freeman, W. T., Tenenbaum, J. B., Finn, C., and Wu, J. Reasoning about physical interactions with object-oriented prediction and planning. In *International Conference on Learning Representations*, 2019.
- Kingma, D. P. and Ba, J. Adam: A method for stochastic optimization. In Bengio, Y. and LeCun, Y. (eds.), *3rd International Conference on Learning Representations, ICLR 2015, San Diego, CA, USA, May 7-9, 2015, Conference Track Proceedings*, 2015. URL <http://arxiv.org/abs/1412.6980>.
- Lee, A. X., Zhang, R., Ebert, F., Abbeel, P., Finn, C., and Levine, S. Stochastic adversarial video prediction. *arXiv preprint arXiv:1804.01523*, 2018.
- Nair, S. and Finn, C. Hierarchical foresight: Self-supervised learning of long-horizon tasks via visual subgoal generation. *arXiv preprint arXiv:1909.05829*, 2019.
- Rubinstein, R. Y. and Kroese, D. P. *The Cross Entropy Method: A Unified Approach To Combinatorial Optimization, Monte-Carlo Simulation (Information Science and Statistics)*. Springer-Verlag, Berlin, Heidelberg, 2004. ISBN 038721240X.
- Singh, A., Yang, L., Hartikainen, K., Finn, C., and Levine, S. End-to-end robotic reinforcement learning without reward engineering. In *Proceedings of Robotics: Science and Systems*, Freiburg im Breisgau, Germany, June 2019. doi: 10.15607/RSS.2019.XV.073.
- Srinivas, A., Jabri, A., Abbeel, P., Levine, S., and Finn, C. Universal planning networks. In *International Conference on Machine Learning (ICML)*, 2018.
- Todorov, E., Erez, T., and Tassa, Y. Mujoco: A physics engine for model-based control. In *2012 IEEE/RSJ International Conference on Intelligent Robots and Systems*, pp. 5026–5033. IEEE, 2012.
- Watter, M., Springenberg, J., Boedecker, J., and Riedmiller, M. Embed to control: A locally linear latent dynamics model for control from raw images. In *Advances in neural information processing systems*, pp. 2746–2754, 2015.
- Wise, M., Ferguson, M., King, D., Diehr, E., and Dymesich, D. Fetch & freight: Standard platforms for service robot applications, 2018. URL <https://fetchrobotics.com/wp-content/uploads/2018/04/Fetch-and-Freight-Workshop-Paper.pdf>.
- Xie, A., Ebert, F., Levine, S., and Finn, C. Improvisation through physical understanding: Using novel objects as tools with visual foresight. *arXiv preprint arXiv:1904.05538*, 2019.
- Xu, D., Nair, S., Zhu, Y., Gao, J., Garg, A., Fei-Fei, L., and Savarese, S. Neural task programming: Learning to generalize across hierarchical tasks. In *2018 IEEE International Conference on Robotics and Automation (ICRA)*, pp. 1–8. IEEE, 2018.
- Ye, Y., Gandhi, D., Gupta, A., and Tulsiani, S. Object-centric forward modeling for model predictive control. *arXiv preprint arXiv:1910.03568*, 2019.
- Yu, T., Shevchuk, G., Sadigh, D., and Finn, C. Unsupervised visuomotor control through distributional planning networks. In *Proceedings of Robotics: Science and Systems*, Freiburg im Breisgau, Germany, June 2019. doi: 10.15607/RSS.2019.XV.020.
- Zagoruyko, S., Labb, Y., Kalevatykh, I., Laptev, I., Carpentier, J., Aubry, M., and Sivic, J. Monte-carlo tree search for efficient visually guided rearrangement planning, 2019.
- Zhu, Y., Wang, Z., Merel, J., Rusu, A., Erez, T., Cabi, S., Tunyasuvunakool, S., Kramár, J., Hadsell, R., de Freitas, N., et al. Reinforcement and imitation learning for diverse visuomotor skills. In *Proceedings of Robotics: Science and Systems*, Pittsburgh, Pennsylvania, June 2018. doi: 10.15607/RSS.2018.XIV.009.

A. GEECO Architecture

In this section, we present additional details regarding the architecture and training hyper-parameters of GEECO and all its ablations.

A.1. Hyper-parameters

Observation Buffer. The observation buffer consists of pairs (I_j, \mathbf{x}_j) , $j \in [t - K + 1, \dots, t]$ of images I_j and proprioceptive features \mathbf{x}_j representing the K most recent observations of the model up to the current time step t . The images are RGB with a resolution of 256×256 and the proprioceptive feature is a vector of length seven containing the angles of the robot’s seven joints at the respective time step. We have experimented with frame buffer sizes $K \in \{2, 4, 6, 8\}$. Buffer sizes smaller than four result in too coarse approximations of dynamics (because velocities have to be inferred from just two time steps) and consequently in lower controller performance. However, controller performance also does not seem to improve with buffer sizes greater than four. We assume that in our scenarios, four frames are sufficient to capture the robot’s motions accurately enough, which is in line with similar experiments in prior work (James et al., 2017). Therefore, we keep the buffer hyper-parameter $K = 4$ fixed in all our experiments. At the start of the execution of the controller, we pad the observation buffer to the left with copies of the oldest frame, if there are less than K pairs in the buffer assuming that the robot is always starting from complete rest.

Convolutional Encoder. All convolutional encoders used in the GEECO architecture have the same structure, which is outlined in table 4. However, the parameters between the convolutional encoders are not shared. The rationale behind this decision is that the different stacks of convolutions are processing semantically different inputs: ψ_{OBS} processes raw RGB observations, ψ_{DYN} processes dynamic images representing the most recent motion captured in the observation buffer and ψ_{DIFF} processes the dynamic image difference between the current observation and the target image.

LSTM Decoder. The spatial feature maps $\psi_{OBS}(I_t)$, $\psi_{DYN}(\hat{\rho}(I_{t-K+1}, \dots, I_t))$, $\psi_{DIFF}(\hat{\rho}(I_t, I_T))$ obtained from the convolutional encoders are concatenated to the proprioceptive feature \mathbf{x}_t containing the current joint angles for the robot’s 7 DoF. This concatenated tensor forms the state representation \mathbf{s}_t , which, in the full model GEECO $_{\mathcal{F}}$, has a shape of $2 \times 2 \times (256 + 256 + 7 + 256)$. The state is subsequently fed into an LSTM (cf. fig. 3). The LSTM has a hidden state \mathbf{h} of size 128 and produces an output vector \mathbf{o}_t of the same dimension at each time step. As shown in prior work (James et al., 2017), maintaining an internal state in the network is crucial for performing multi-stage tasks such as pick-and-place.

LAYER	FILTERS	KERNEL	STRIDE	ACTIVATION
CONV1	32	3	1	RELU
CONV2	48	3	2	RELU
CONV3	64	3	2	RELU
CONV4	128	3	2	RELU
CONV5	192	3	2	RELU
CONV6	256	3	2	RELU
CONV7	256	3	2	RELU
CONV8	256	3	2	RELU

Table 4. The convolutional encoders used in GEECO all share the same structure of eight consecutive layers of 2D convolutions. They take as inputs RGB images with a resolution of 256×256 and return spatial feature maps with a shape of $2 \times 2 \times 256$.

At the beginning of each task, i.e. when the target image I_T is set and before the first action is executed, the LSTM state is initialised with a zero vector. The output \mathbf{o}_t at each timestep is passed through a fully connected layer $\phi(\cdot)$ with 128 neurons and a RELU activation function. This last-layer feature $\phi(\mathbf{o}_t)$ is finally passed through four parallel, fully-connected decoding heads without an activation function to obtain the command vectors and the auxiliary position estimates for the object and the end effector as described in table 5.

HEAD	UNITS	OUTPUT
$\hat{\mathbf{u}}_{\Delta EE}$	3	change in EE position $(\Delta x, \Delta y, \Delta z)$
$\hat{\mathbf{u}}_{GRP}$	3	logits for {open, noop, close}
$\hat{\mathbf{q}}_{EE}$	3	absolute EE position (x, y, z)
$\hat{\mathbf{q}}_{POS}$	3	absolute OBJ position (x, y, z)

Table 5. The output heads of the LSTM decoder regressing to the commands and auxiliary position estimates.

Training Details. We train all versions of GEECO with a batch size of 32 for 300k gradient steps using the Adam optimiser (Kingma & Ba, 2015) with a start learning rate of $1e-4$. One training run takes approximately 48 hours to complete using a single NVIDIA GTX 1080 Ti with 11 GB of memory.

Execution Time. Running one simulated trial with an episode length of eight seconds takes about ten seconds for any version of GEECO using a single NVIDIA GTX 1080 Ti. This timing includes the computational overhead for running and rendering the physics simulation resulting in a lower-bound estimate of GEECO’s control frequency at 20 Hz. This indicates that our model is nearly real-time capable of continuous control without major modifications.

A.2. Ablation Details

GEECO_C GEECO_C, which is presented in fig. 7, is the simplest ablation of the goal-conditioned controller where the feature obtained from the target image is simply concatenated to the state representation. Since the observation buffer is not compressed into a dynamic image via $\hat{\rho}(\cdot)$, it is processed slightly differently in order to retain information about the motion dynamics. For each pair (I_j, \mathbf{x}_j) , $j \in [t - K + 1, \dots, t]$ containing an observed image and a proprioceptive feature at time step j , the corresponding state representation \mathbf{s}_j is computed and fed into the LSTM which, in turn, updates its state. However, only after all K pairs of the observation buffer have been fed, the command outputs are decoded from the LSTM’s last output vector. This delegates the task of inferring motion dynamics to the LSTM as it processes the observation buffer.

GEECO_R GEECO_R, which is presented in fig. 8, is almost identical to GEECO_C except for the fact that a *residual* target encoding is used instead of a *constant* one. The residual feature is the difference $\psi_{OBS}(I_T) - \psi_{OBS}(I_j)$, $j \in [t - K + 1, \dots, t]$ and should tend towards zero as the observation I_j approaches the target image I_T . Since the same encoder ψ_{OBS} is used for observation and target image, this architecture should encourage the formation of a feature space which captures the difference between an observation and the target image in a semantically meaningful way. The K pairs in the observation buffer are processed like in GEECO_C.

GEECO_D GEECO_D, which is presented in fig. 9, uses the dynamic image operator $\hat{\rho}(\cdot)$ to compute the difference between each observed frame I_j , $j \in [t - K + 1, \dots, t]$ and the target image I_T as opposed to GEECO_C which just represents the target frame as a constant feature. Since the *dynamic difference* $\rho(I_t, I_T)$ is semantically different from a normal RGB observation, it is processed with a dedicated convolutional encoder ψ_{DIFF} and the resulting feature is concatenated to the state representation \mathbf{s}_t . In order to also capture motion dynamics, the observation buffer is processed sequentially like in GEECO_{C/R} before a control command is issued.

B. Visual Foresight Baseline

In this section, we explain all hyper-parameters which have been used during training and evaluation of the Visual Foresight model (Ebert et al., 2018).

Video Predictor. We use the official implementation⁴ of Stochastic Adversarial Video Prediction (Lee et al., 2018) as the video prediction backbone of Visual Foresight. We have not been able to fit the model at a resolution of $256 \times$

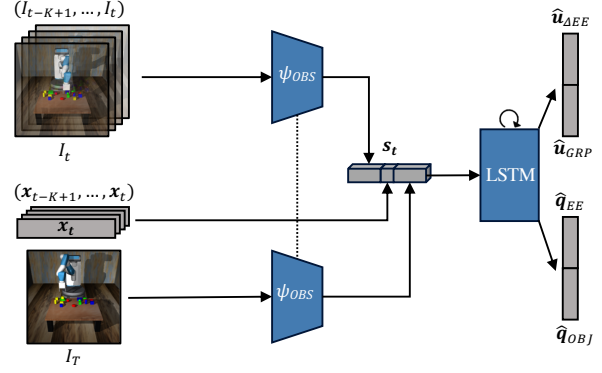


Figure 7. Model architecture of GEECO_C. The same convolutional encoder ψ_{OBS} is used to encode RGB observations I_t and the target frame I_T . The features obtained are concatenated with \mathbf{x}_t to form the state representation \mathbf{s}_t .

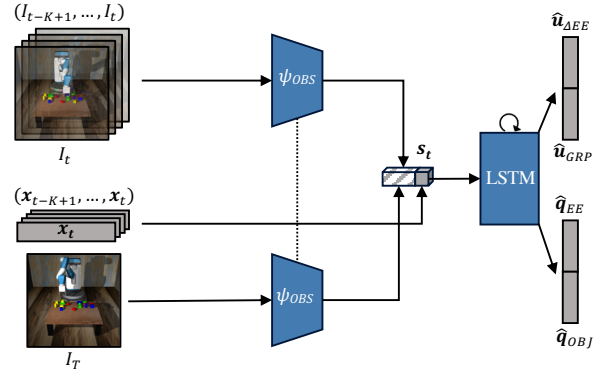


Figure 8. Model architecture of GEECO_R. The same encoder ψ_{OBS} is used for RGB observations I_t and the target frame I_T . For each observed image I_t , the residual feature w.r.t. to the target image I_T is computed as $\psi_{OBS}(I_T) - \psi_{OBS}(I_t)$, indicated by the striped box in \mathbf{s}_t .

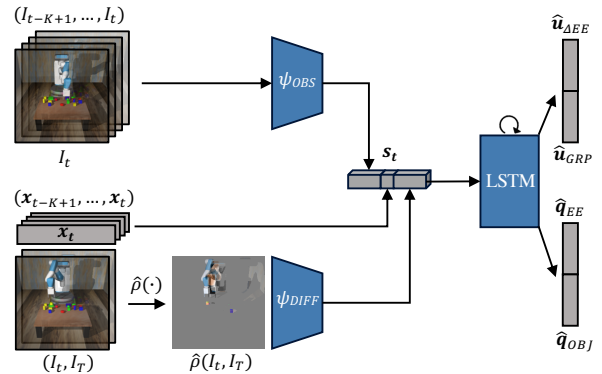


Figure 9. Model architecture of GEECO_D. For each image I_t in the observation buffer, the *dynamic difference* to the target image I_T is computed using $\hat{\rho}(\cdot)$. The difference image $\hat{\rho}(I_t, I_T)$ is encoded with ψ_{DIFF} before being concatenated to \mathbf{s}_t .

⁴<https://github.com/alexlee-gk/video-prediction>

256 on a single GPU with 11 GB of memory. Hence, we adjusted the image resolution of the video predictor to 128×128 pixels. We use SAVP’s hyper-parameter set which is reported for the BAIR robot pushing dataset (Ebert et al., 2017) since those scenarios resemble our training setup most closely. We report the hyper-parameter setup in table 6.

PARAMETER	VALUE	DESCRIPTION
scale_size	128	image resolution
use_state	True	use action conditioning
sequence_length	13	prediction horizon
frame_skip	0	use entire video
time_shift	0	use original frame rate
l1_weight	1.0	use L_1 reconstruction loss
kl_weight	0.0	make model deterministic
state_weight	1e-4	weight of conditioning loss

Table 6. Hyper-parameter setup of SAVP. Hyper-parameters not listed here are kept at their respective default values.

Training Details. We train SAVP with a batch size of 11 for 300k gradient steps using the Adam optimiser (Kingma & Ba, 2015) with a start learning rate of 1e-4. One training run takes approximately 72 hours to complete using a single NVIDIA GTX 1080 Ti with 11 GB of memory.

Action Sampling. We use CEM (Rubinstein & Kroese, 2004) as in the original VFS paper (Ebert et al., 2018) to sample actions which bring the scene closer to a desired target image under the video prediction model. We set the *planning horizon* of VFS to the prediction length of SAVP, $P = 13$. The action space is identical to the one used in GEECO and consists of a continuous vector representing the position change in the end effector $\mathbf{u}_{\Delta EE} \in \mathbb{R}^3$ and a discrete command for the gripper $\mathbf{u}_{GRP} \in \{-1, 0, 1\}$. Once a target image has been set, we sample action sequences of length P according to the following eqs. (4) and (5):

$$\mathbf{u}_{\Delta EE}^{1:P} \sim \mathcal{N}(\mu, \Sigma) \quad (4)$$

$$\mathbf{u}_{GRP}^{1:P} \sim \mathcal{U}\{-1, 0, 1\} \quad (5)$$

where $\mathcal{N}(\mu, \Sigma)$ is a multi-variate Gaussian distribution and $\mathcal{U}\{-1, 0, 1\}$ is a uniform distribution over the gripper states. For each planning step, we run CEM for four iterations drawing 200 samples at each step and re-fit the distributions to the ten best action sequences according to the video predictor, i.e. the action sequences which transform the scene closest to the next goal image. Finally, we execute the best action sequence yielded from the last CEM iteration and re-plan after P steps.

Goal Distance. We use L_2 distance in image space to determine the distance between an image forecast by the video predictor and a target image (cf. (Ebert et al., 2018)).

Since this goal distance is dominated by large image regions (e.g. the robot arm), it is ill suited to capture position differences of the comparatively small objects on the table or provide a good signal when a trajectory is required which is not a straight line. Therefore, we resort to a ‘ground truth bottleneck’ scheme (Nair & Finn, 2019) for a fairer comparison. Instead of providing just a single target image from the end of an expert demonstration, we give the model ten *intermediate target frames* taken every ten steps during the expert demonstration. This breaks down the long-horizon planning problem into multiple short-horizon ones with approximately straight-line trajectories between any two intermediate targets. This gives an upper-bound estimate of VFS’s performance, if it had access to a perfect keyframe predictor splitting the long-horizon problem. An example execution of VFS being guided along intermediate target frames is presented in fig. 10.

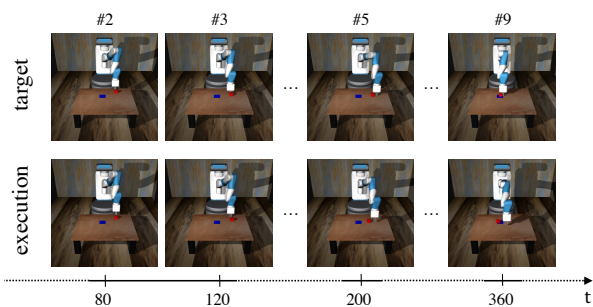


Figure 10. An execution of VFS with the ‘ground truth bottleneck’ scheme. The top row depicts intermediate target images from an expert demonstration. The bottom row shows the corresponding state of execution via VFS at time step t .

Execution Time. To account for VFS’s sampling-based nature and the guided control process using intermediate target images, we give VFS some additional time to execute a task during test time. We set the total test episode length to 400 time steps as opposed to 200 used during the evaluation of GEECO. VFS is given 40 time steps to ‘complete’ each sub-goal presented via the ten intermediate target images. However, the intermediate target image is updated to the next sub-goal strictly every 40 time steps, irrespective of how ‘close’ the controller has come to achieving the previous sub-goal. Running one simulated trial with an episode length of 16 seconds takes about ten minutes using a single NVIDIA GTX 1080 Ti. This timing includes the computational overhead for running and rendering the physics simulation. While this results in an effective control frequency of 0.7 Hz, a like-for-like comparison between VFS and GEECO can not be made in that regard because we have not tuned VFS for runtime efficiency in our scenarios. Potential speedups can be gained from lowering the image resolution and frame rate of the video predictor, predicting shorter time horizons and pipelining the re-planning

procedure in a separate thread. However, the fundamental computational bottlenecks of visual MPC can not be overcome with hyper-parameter tuning: Action-conditioned video prediction remains an expensive operation for dynamics forecasting although pixel-level prediction accuracy is presumably not needed to control a robot. Additionally, the action sampling process is a separate part of the model which requires tuning and trades off accuracy versus execution time. In contrast to that, GEECO provides a compelling alternative by reducing the action computation to a single forward pass through the controller network.

C. Additional Experiments

In this section we present two additional experiments: Firstly, we compare all versions of GEECO with an unconditioned visuomotor controller on the unambiguous scenarios GOAL1CUBE1 in appendix C.1. Secondly, we analyse how well GEECO transfers to new scenarios featuring more objects if it had only been trained seeing one cube and one target pad. We present the results of this generalisation study in appendix C.2

C.1. E2EVMC Baseline

We compare GEECO to E2EVMC (James et al., 2017), an unconditioned visuomotor controller, which we have implemented according to the original paper. For a fair comparison, we restrict training and evaluation to the unambiguous scenarios GOAL1CUBE1. We train E2EVMC exactly like GEECO (cf. appendix A.1: Training Details) and select the best model snapshots according to the loss on the respective validation sets. We present the model comparison in table 7.

MODEL	GOAL1CUBE1		GOAL1CUBE1		
	REACH [%]	PUSH [%]	REACH [%]	PICK [%]	PLACE [%]
RAND	6	2	6	2	0
E2EVMC	98	64	98	78	68
GEECO _C	98	64	98	84	56
GEECO _R	98	42	94	58	47
GEECO _D	98	68	98	89	54
GEECO _F	100	55	96	80	79

Table 7. Comparison of pushing and pick-and-place performance of all versions of GEECO with E2EVMC on GOAL1CUBE1.

The results reveal that the different goal-conditioning schemes do not always improve controller performance, especially in the case of GEECO_R. We conjecture that using *residual encoding*, no meaningful feature space can be learned when the goal images are not diverse enough (i.e. always showing a red cube on a blue target pad). However, even in unambiguous scenarios, using dynamic images adds

a small performance increase, demonstrated by GEECO_D for pushing and by GEECO_F for pick-and-place tasks.

C.2. Generalisation Study

In this experiment we train all versions of GEECO exclusively tasks from the GOAL1CUBE1 scenario. Despite the fact that only unambiguous setups are shown, i.e. the red cube was always supposed to be pushed or dropped onto the blue target pad, a *versatile* controller should be able to transfer at least some basic knowledge about the skill it is trained on to new scenarios. Basic skill knowledge could encompass behaviours like going towards the desired object to move, grasping or pushing an object and resting once the object has reached its designated target area. We present the results for GEECO’s generalisation capabilities on pushing tasks in table 8 and on pick-and-place tasks in table 9.

The results show that GEECO ablations using dynamic image representations (\mathcal{D} , \mathcal{F}) consistently outperform the ‘RGB-only’ ablations (\mathcal{C} , \mathcal{R}). This is in line with the results presented in section 4 where \mathcal{D} and \mathcal{F} also retained high task performances in heavily cluttered environments. GEECO_R performs worst on average, especially on the pick-and-place tasks. This is in line with results from appendix C.1 adding further evidence that diverse goal images are needed during training to learn a meaningful feature space using residual target encoding. In contrast to that, the consistently high performance of GEECO_F (especially in the GOAL2CUBE1 and GOAL2CUBE2 scenarios) hints at the utility of dynamic image in generalising to new scenarios by adding inductive biases about geometry and motion dynamics directly to the model architecture.

D. Qualitative Results

We refer the reader to the supplementary video for a qualitative demonstration of the performance of GEECO found here: <https://youtu.be/zn1P0r9zCU>. Specifically, we present examples depicting common success and failure modes of our model as well as a side-by-side execution comparison to VFS.

E. Release of Source Code and Data

Each dataset of expert demonstrations for each of our scenarios is approximately 100 GB in size containing 4,000 videos at a resolution of 256×256 pixels, fully annotated with ground-truth robot commands, proprioception and world state information. We will make all data publicly available. We will also release source code for model implementation, Gym environments and evaluation scripts for full reproducibility of all results.

MODEL	GOAL1CUBE2		GOAL2CUBE1		GOAL2CUBE2	
	REACH [%]	PUSH [%]	REACH [%]	PUSH [%]	REACH [%]	PUSH [%]
RAND	4	12	7	8	0	12
GEECO _C	39 (-58)	11 (-60)	51 (-46)	11 (-56)	42 (-57)	13 (-69)
GEECO _R	52 (-48)	12 (-55)	66 (-33)	8 (-65)	36 (-63)	12 (-43)
GEECO _D	43 (-56)	17 (-65)	50 (-49)	20 (-67)	59 (-41)	16 (-54)
GEECO _F	58 (-40)	15 (-52)	93 (-7)	26 (-60)	56 (-43)	21 (-21)

Table 8. Pushing performance for models trained on GOAL1CUBE1 data and tested on the three remaining basic scenarios featuring more objects. The numbers in brackets show the performance difference to a model which has been trained on the same scenario (cf. table 1). Best performance and lowest drop in performance are bold-faced in each column.

MODEL	GOAL1CUBE2			GOAL2CUBE1			GOAL2CUBE2		
	REACH [%]	PICK [%]	PLACE [%]	REACH [%]	PICK [%]	PLACE [%]	REACH [%]	PICK [%]	PLACE [%]
RAND	7	1	0	7	0	0	8	1	0
GEECO _C	46 (-23)	38 (± 0)	24 (+4)	60 (-37)	23 (-58)	6 (-58)	30 (-23)	10 (-12)	1 (-5)
GEECO _R	44 (-47)	21 (-41)	22 (-17)	44 (-52)	18 (-55)	7 (-40)	19 (-68)	3 (-51)	2 (-31)
GEECO _D	47 (-47)	37 (-34)	22 (-22)	74 (-22)	22 (-51)	4 (-35)	36 (-62)	6 (-74)	1 (-40)
GEECO _F	45 (-49)	32 (-24)	29 (-12)	94 (-5)	52 (-37)	17 (-34)	52 (-42)	33 (-53)	8 (-23)

Table 9. Pick-and-place performance for models trained on GOAL1CUBE1 data and tested on the three remaining basic scenarios featuring more objects. The numbers in brackets show the performance difference to a model which has been trained on the same scenario (cf. table 2). Best performance and lowest drop in performance are bold-faced in each column.